Supplementary Information

Tissue Factor-Specific Ultra-Bright SERRS Nanostars for Raman Detection of Pulmonary Micrometastases

Tapas R. Nayak[1Δ], Chrysafis Andreou[1Δ], Anton Oseledchyk[1], Warren D. Marcus[2], Hing C. Wong[2], Joan Massagué[3] and Moritz F. Kircher[1, 4, 5, *]

[1]Department of Radiology, Memorial Sloan Kettering Cancer Center, New York, NY, 10065, USA;

[2]Altor BioScience Corporation, Miramar, FL, 33025, USA

[3]Cancer Biology and Genetics Program, Memorial Sloan Kettering Cancer Center, New York, NY, 10065, USA;

[4]Center for Molecular Imaging and Nanotechnology (CMINT), Memorial Sloan Kettering Cancer Center, New York, NY, 10065, USA

[5]Department of Radiology, Weill Cornell Medical College, New York, New York 10065, USA

[Δ]These authors contributed equally to this work.

[*]Corresponding author email: kircherm@mskcc.org.

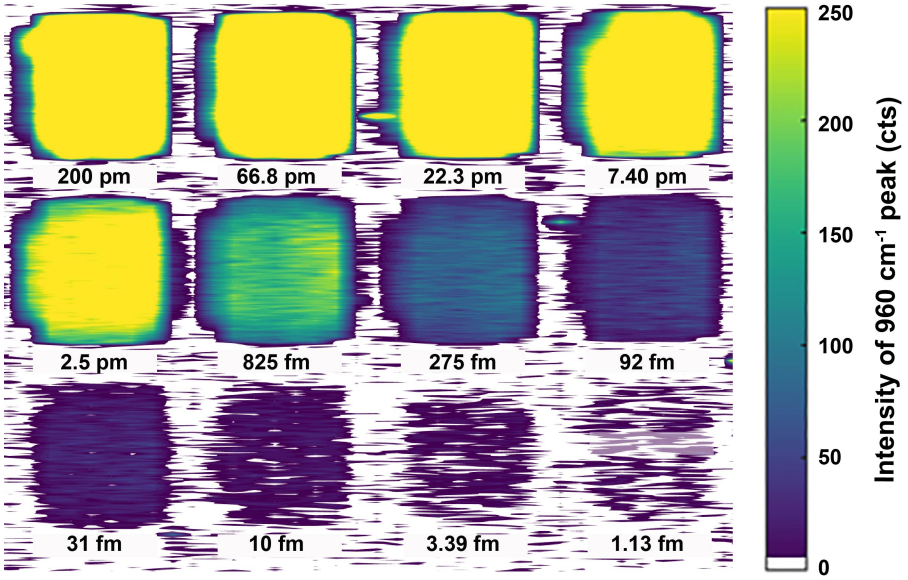

Figure S1: Raman intensity of varying concentration of SERRS-NPs measured in a 384 well-plate using the same settings as for *in vivo* imaging. The limit of detection was found to be approximately 10 fm.

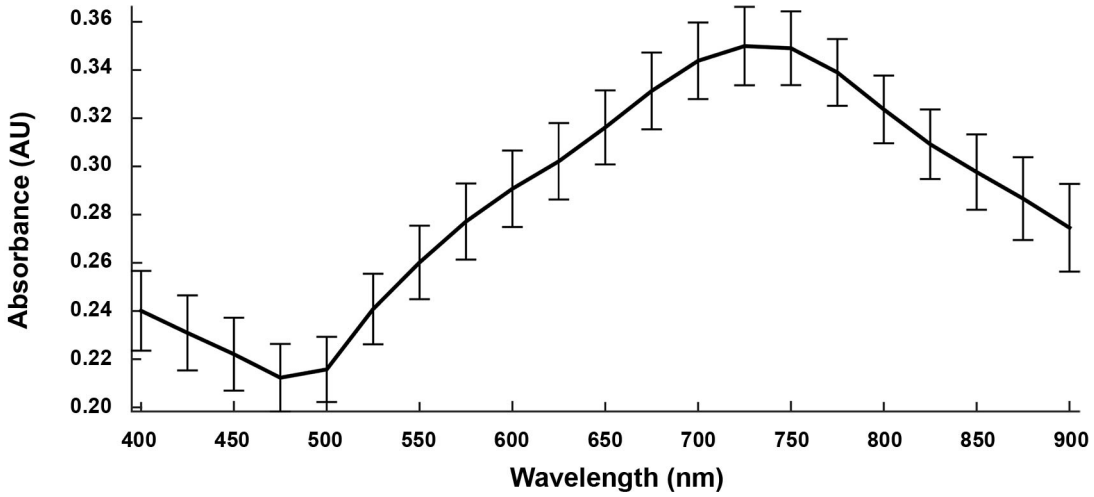

Figure S2: Absorbance spectrum of SERRS-NPs. The maximum absorbance is at 740 nm, with high absorbance in the wavelength of the Raman interrogation laser (785 nm).

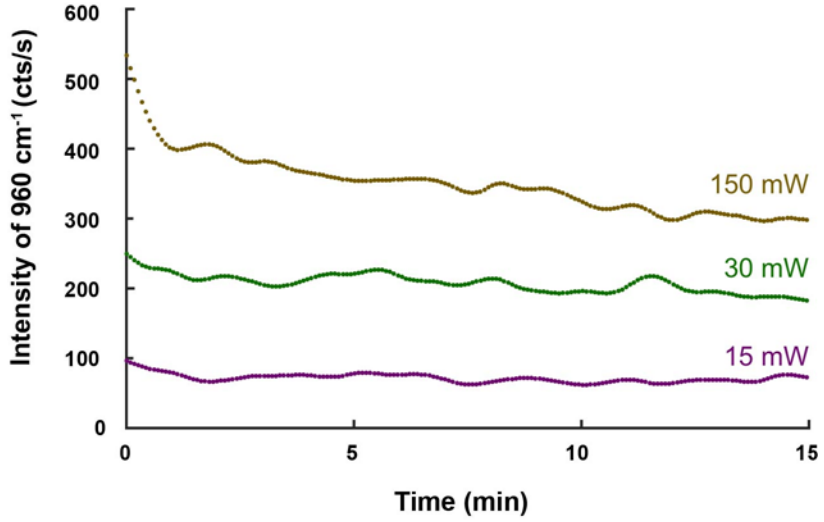

Figure S3: Photo-stability of SERRS-NPs. Intensity of the 960 cm^{-1} peak *vs.* time, with continuous laser illumination. For high laser power (> 30 mW) the SERRS-NPs decrease in intensity over the course of minutes. Raman imaging with our imaging parameters requires milliseconds per each point.

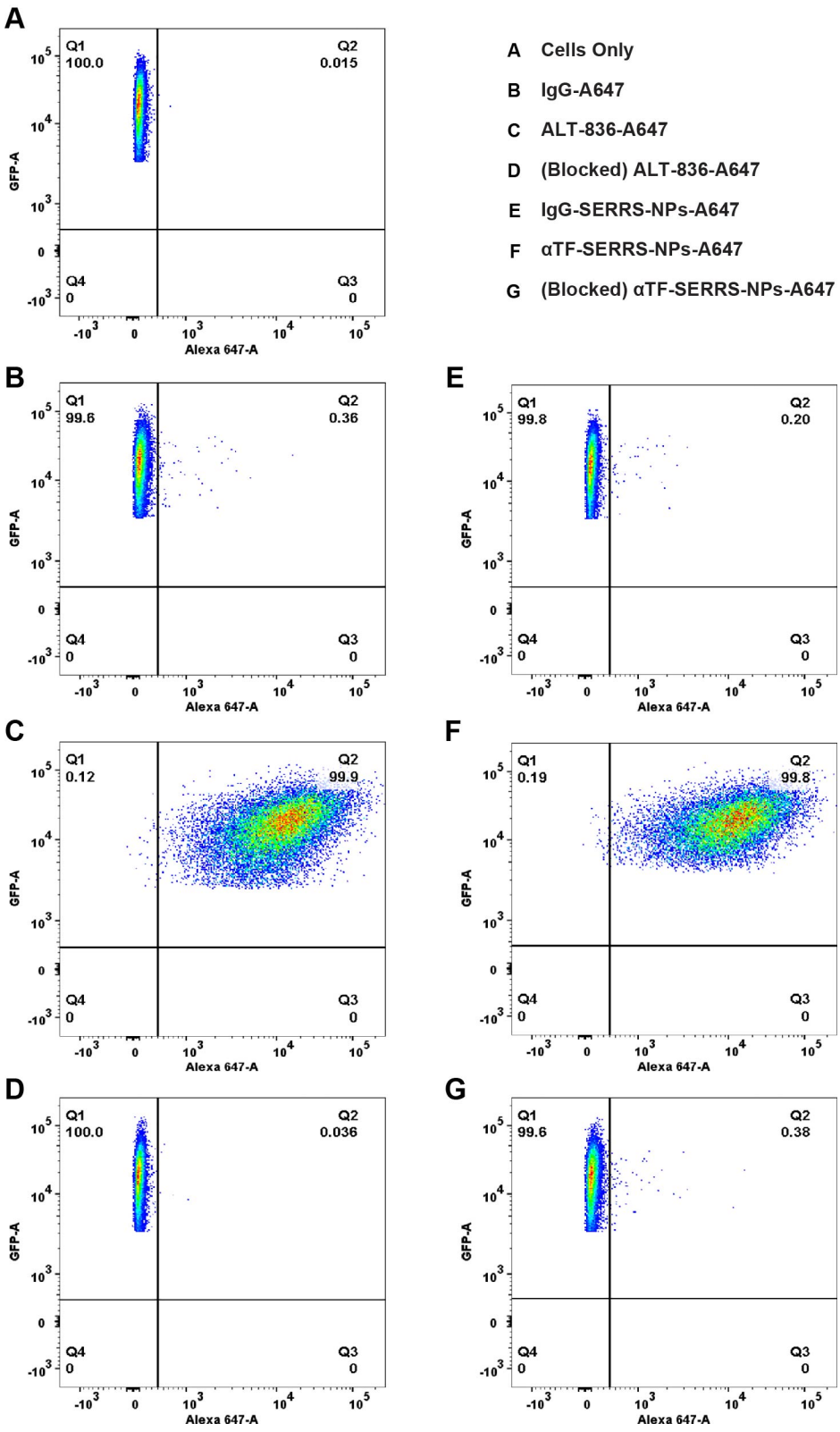

Figure S4: Flow cytometry analysis for binding affinity and TF specificity of ALT-836-A647 and αTF-SERRS-NPs-A647 in comparison to isotype and blocking controls.

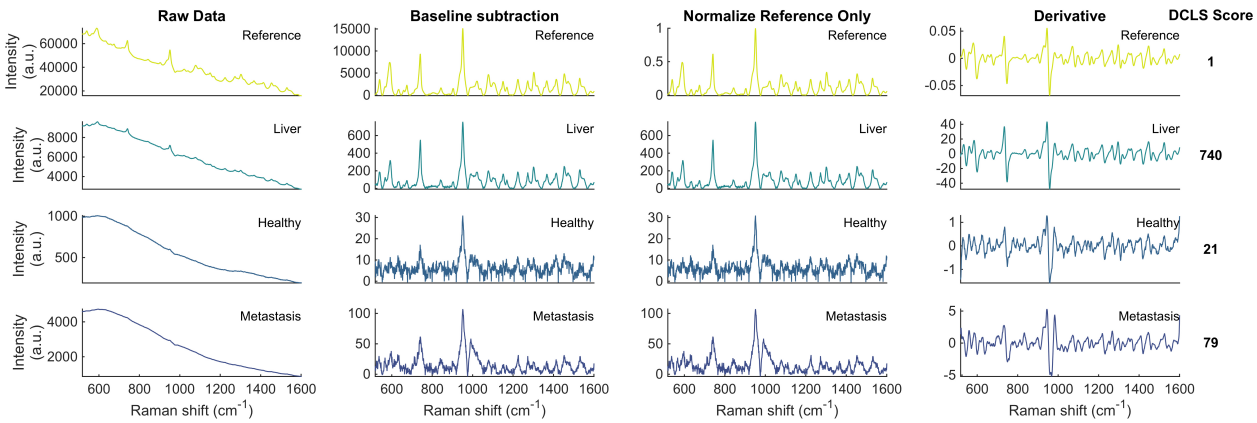

Figure S5: DCLS analysis. The Raman images were generated based on the direct classical least squares algorithm presented here. A reference spectrum (top row) was collected from a pure population of SERRS-NPs. Average spectra collected from liver, healthy lung, and metastatic lung are shown for comparison. The raw spectra (column 1) are subjected to baseline subtraction (Whittaker, λ=200 cm^{-1}) to remove the fluorescence background (column 2). Only the reference spectrum is normalized (column 3), so that the final predicted DCLS scores correspond to the magnitude of the spectra. Finally, the spectra are differentiated (column 4) and subjected to the DCLS analysis to obtain the final DCLS scores (column 5).

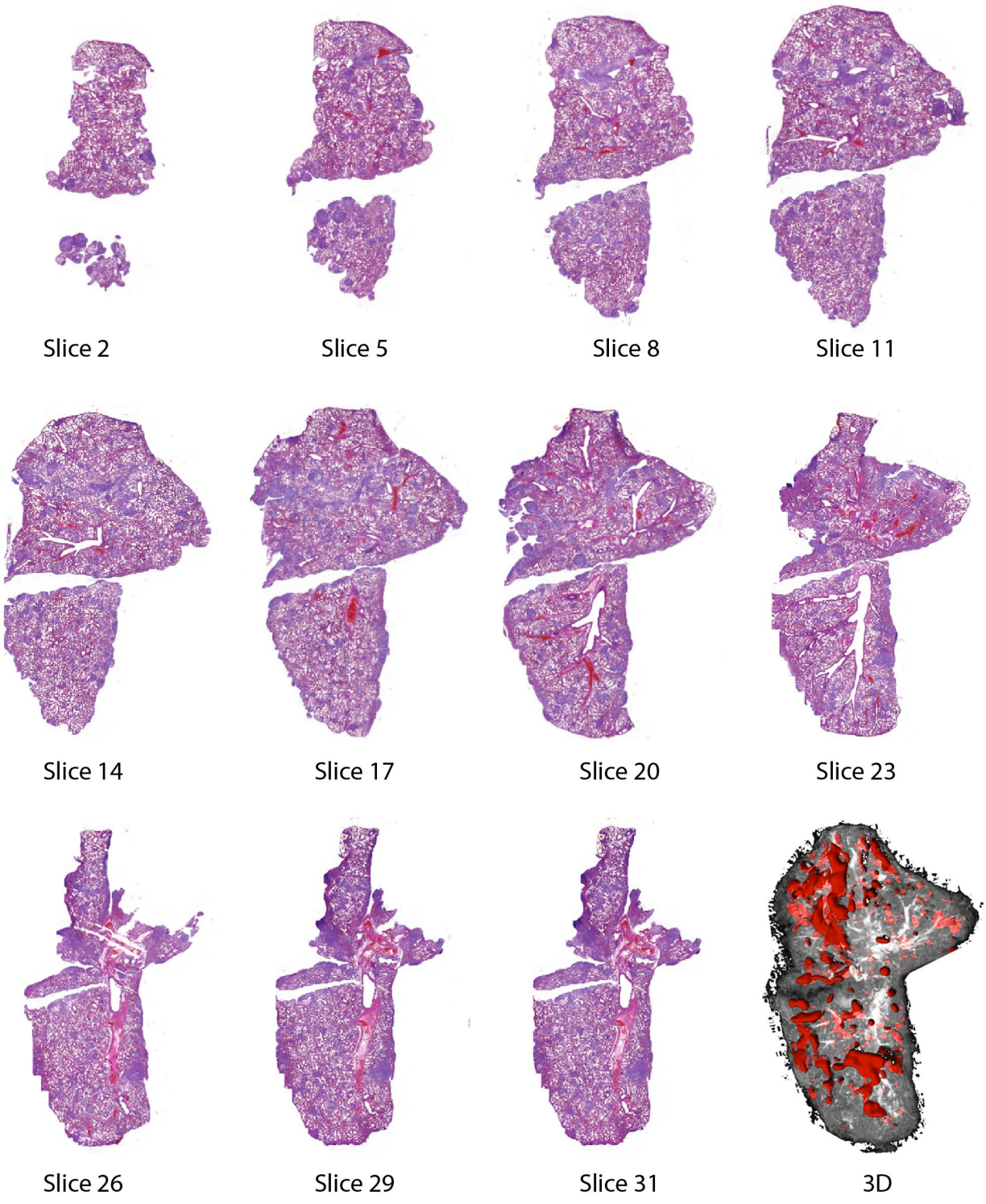

Figure S6: Histological analysis of a lung with metastatic lesions. H&E staining of sliced fixed tissue – the gold standard of histological validation – fails to provide an accurate representation of the tumor burden in the case of multiple microscopic metastases. Thin tissue slices (5 µm), taken 30 µm apart (11 representative slices shown here) show distinct tumor distribution for specific planes of section, missing tumor lesions which could be seen in the Raman map. To remedy this, a 3D reconstruction of the lung was produced based on 40 such tissue slices.